

See discussions, stats, and author profiles for this publication at: <https://www.researchgate.net/publication/236062908>

H₃O₂ Bridging Ligand in a Metal–Organic Framework. Insight into the Aqua–Hydroxo <–> Hydroxyl Equilibrium: A Combined Experimental and Theoretical Study

ARTICLE in JOURNAL OF THE AMERICAN CHEMICAL SOCIETY · MARCH 2013

Impact Factor: 12.11 · DOI: 10.1021/ja4005046 · Source: PubMed

CITATIONS

22

READS

148

6 AUTHORS, INCLUDING:



Richard Fernando D'vries

University of São Paulo

21 PUBLICATIONS 152 CITATIONS

SEE PROFILE



Victor Antonio de la Peña O'Shea

Madrid Institute for Advanced Studies

75 PUBLICATIONS 1,255 CITATIONS

SEE PROFILE



Enrique Gutiérrez-Puebla

Instituto de Ciencia de Materiales de Madrid

346 PUBLICATIONS 6,103 CITATIONS

SEE PROFILE



Angeles Monge

Spanish National Research Council

441 PUBLICATIONS 6,747 CITATIONS

SEE PROFILE

H₃O₂ Bridging Ligand in a Metal–Organic Framework. Insight into the Aqua-Hydroxo ↔ Hydroxyl Equilibrium: A Combined Experimental and Theoretical Study

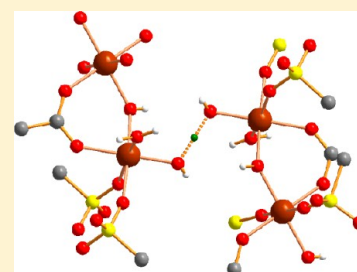
Richard F. D’Vries,[†] Victor A. de la Peña-O’Shea,[‡] Natalia Snejko,[†] Marta Iglesias,[†] Enrique Gutiérrez-Puebla,[†] and M. Angeles Monge^{*,†}

[†]Department of New Architectures in Materials Chemistry, Instituto de Ciencia de Materiales de Madrid, ICMN-CSIC, c/Sor Juana Inés de la Cruz, 3, 28049 Madrid, Spain

[‡]Thermochemical Process Group, Instituto Madrileño de Estudios Avanzados en Energía (IMDEA Energía), c/Tulipán s/n, 28933 Móstoles, Spain

S Supporting Information

ABSTRACT: A metal–organic framework (MOF) bearing the aqua-hydroxo species (O_2H_3)[−] in the framework, as well as the processes that govern the equilibrium aqua-hydroxo (O_2H_3)[−] ↔ hydroxyl (OH) in Sc-MOFs, are studied experimentally and theoretically. Computational studies were employed to determine the relative energies for the two compounds that coexist under certain hydrothermal conditions at pH < 2.8. The thermodynamically more stable $[\text{Sc}_3(3,5\text{-DSB})_2(\mu\text{-O}_2\text{H}_3)(\mu\text{-OH})_2(\text{H}_2\text{O})_2]$ (from now on, (O_2H_3)Sc-MOF; 3,5-DSB = 3,5-disulfobenzoic acid) was obtained as a pure and stable phase. It was impossible to isolate $[\text{Sc}_3(3,5\text{-DSB})_2(\mu\text{-OH})_3(\text{H}_2\text{O})_4]$ as a pure phase, as it turned out to be the precursor of (O_2H_3)Sc-MOF. Additionally, a third compound that appears at pH between 3.5 and 4, $[\text{Sc}_3(3,5\text{-DSB})(\mu\text{-OH})_6(\text{H}_2\text{O})]$ and a fourth, $[\text{Sc}(3,5\text{-DSB})(\text{Phen})(\text{H}_2\text{O})](\text{H}_2\text{O})$, in whose formula neither OH groups nor H_3O_2^- anions appear, are reported for comparative purposes. A study of the (O_2H_3)Sc-MOF electronic structure, and some heterogeneous catalytic tests in cyanosilylation of aldehydes reactions, are also reported.



■ INTRODUCTION

The observed increasing interest in chemistry involving the scandium cation is mainly due to the use of its compounds as catalysts in organic syntheses,¹ although scandium compounds have many other useful properties. Sc^{III} cation seems to be an interesting connector in the design of new coordination polymer architectures,² not only for its foreseen and controllable mode of coordination, but also for its chemical characteristics, such as Lewis acidity, that make Sc-containing materials very attractive as heterogeneous catalysts. Relatively few examples of Sc^{III}-based metal–organic frameworks (MOFs) have been reported in the literature.³ The particular features of these compounds range from catalytic reactions like epoxidation reaction,^{3b} Friedel–Craft acylations,⁴ and cyanosilylation reaction^{3e} to gas adsorption capacity.^{3c,d,5} It should be noticed that there are not really many different modes of linkages in Sc-MOFs. In various Sc-MOFs, the cations are linked to each other, apart from via the corresponding carboxylate or sulfonate oxygen atoms, through μ -OH groups, forming dimers.⁶ In some Sc-MOFs there exists also the Sc_3O moiety.^{3d,7} There has been a growing interest in developing MOFs derived from Sc^{III} using the $[\text{Sc}_2(\mu_2\text{-OH})]$ fragment as a potential building block.^{6a} The first μ_2 -OH-bridged Sc^{III}-based MOF, $[\text{Sc}_2(\mu_2\text{-OH})(\text{O}_2\text{C}_2\text{H}_4\text{CO}_2)_{2.5}]_\infty$, showed Lewis acid catalytic activity, combined with high thermal stability. A scandium croconate polynuclear complex, whose supramolecular net comprises μ_2 -OH and μ_4 -OH bridges inside

Sc₇O₃₂ heptanuclear clusters, has also been reported.⁸ Following our interest in the study of the influence of $[\mu\text{-OH}]$ species on the structure formation, and taking into account that some transition metal complexes dimers are formed via aqua-hydroxo species,⁹ we explored the synthesis in the system Sc^{III}/3,5-DSB (DSB = disulfobenzoic acid) at low pH values. In order to get an extended net, the chosen linker was 3,5-DSB, a multi-topic ligand with two sulfonate groups that confer acidity to the reaction medium and one carboxylate group. The results of the study are presented in this paper. We report the first MOF bearing the aqua-hydroxo species in the framework, as well as the experimental and theoretical conditions that govern the equilibrium aqua-hydroxo (O_2H_3)[−] ↔ hydroxyl (OH) in Sc-MOFs. Additionally, a third compound that appears between pH 3.5 and 4, and a fourth, in which by using the chelate Phen ligand two of the Sc coordination sites are blocked and in whose formula neither OH[−] group nor H_3O_2^- anions appear, are also reported for comparison. A study of the (O_2H_3)Sc-MOF electronic structure, and some heterogeneous catalytic tests in cyanosilylation of aldehydes reactions, are also reported.

Received: January 16, 2013

Published: March 19, 2013

■ EXPERIMENTAL SECTION

General Information. All reagents and solvents employed were commercially available and used as supplied without further purification: 3,5-disulfobenzoic acid, disodium salt (98%, Sigma-Aldrich); scandium chloride hexahydrate (99.9%, Strem Chemicals). The IR spectra were recorded from KBr pellets in the range 4000–250 cm^{-1} on a Bruker IFS 66V/S instrument. Thermogravimetric analysis (TGA) and differential thermal analysis (DTA) were performed using a Seiko TG/DTA 320U instrument at temperatures between 25 and 1000 $^{\circ}\text{C}$ in air atmosphere (100 mL/min flow) and a heating rate of 10 $^{\circ}\text{C}/\text{min}$. A Perkin-Elmer CNHS Analyzer 2400 instrument was employed for the elemental analysis. Powder X-ray diffraction (PXRD) patterns were measured with a Bruker D8 diffractometer, with step size of 0.02 $^{\circ}$ and exposure time of 0.5 s/step.

Synthesis. The compounds were synthesized under hydrothermal conditions. The molar composition of the initial reaction mixture was $3,5\text{-DSB}^{3-}:\text{Sc}^{\text{III}}:1727\text{H}_2\text{O}$ for $[\text{Sc}_3(3,5\text{-DSB})_2(\mu\text{-O}_2\text{H}_3)(\mu\text{-OH})_2(\text{H}_2\text{O})_2]$ (from now on, $(\text{O}_2\text{H}_3)\text{Sc-MOF}$), $[\text{Sc}_3(3,5\text{-DSB})_2(\mu\text{-OH})_3(\text{H}_2\text{O})_4]$ (from now on, $(\mu\text{-OH})_3\text{Sc-MOF}$), and $[\text{Sc}_3(3,5\text{-DSB})(\mu\text{-OH})_6(\text{H}_2\text{O})]$ (from now on, $(\mu\text{-OH})_6\text{Sc-MOF}$).

$(\text{O}_2\text{H}_3)\text{Sc-MOF}$ was synthesized by addition of $3,5\text{-DSBNa}_2$ (0.052 g, 0.16 mmol) to a solution of $\text{Sc}(\text{NO}_3)_3 \cdot 6\text{H}_2\text{O}$ (0.05 g, 0.16 mmol, 6 mL of water); an aqueous 1 M solution of sodium hydroxide was added dropwise to adjust the pH to ~ 3.5 . The reaction mixture was magnetically stirred at room temperature for 15 min, placed into a Teflon-lined stainless steel autoclave, and heated at 200 $^{\circ}\text{C}$ for 1 day. After cooling to room temperature, the crystalline product was filtered and washed with water and acetone, with a yield of 67%. Elemental analysis calculated for $\text{C}_{14}\text{H}_{15}\text{O}_{23}\text{S}_4\text{Sc}_3$: C, 21.04; H, 1.76; S, 16.05. Found: C, 21.13; H, 1.65; S, 15.75.

For $(\mu\text{-OH})_3\text{Sc-MOF}$ synthesis, a wide range of conditions (temperature, pH, reaction time) were tested in order to obtain a pure phase. A mixture of $(\text{O}_2\text{H}_3)\text{Sc-MOF}$ and $(\mu\text{-OH})_3\text{Sc-MOF}$ was obtained by addition of $3,5\text{-DSBNa}_2$ (0.052 g, 0.16 mmol) to a solution of $\text{Sc}(\text{NO}_3)_3 \cdot 6\text{H}_2\text{O}$ (0.05 g, 0.16 mmol, 6 mL of water); an aqueous 1 M solution of sodium hydroxide was added dropwise to adjust the pH to ~ 2.8 . The reaction mixture was magnetically stirred at room temperature for 15 min, placed into a Teflon-lined stainless steel autoclave, and heated at 220 $^{\circ}\text{C}$ at different reaction times. Due to the small amount of compound produced, this product could be only detected by powder X-ray diffraction; a few crystals of the $(\text{OH})_3\text{Sc-MOF}$ were hand-selected and analyzed by single-crystal X-ray diffraction and IR spectroscopy.

$(\mu\text{-OH})_6\text{Sc-MOF}$ was synthesized by addition of $3,5\text{-DSBNa}_2$ (0.052 g, 0.16 mmol) to a solution of $\text{Sc}(\text{NO}_3)_3 \cdot 6\text{H}_2\text{O}$ (0.05 g, 0.16 mmol, 6 mL water); an aqueous 1 M solution of sodium hydroxide was added dropwise to adjust the pH to ~ 4 . The reaction mixture was magnetically stirred at room temperature for 15 min, placed into a Teflon-lined stainless steel autoclave, and heated at 200 $^{\circ}\text{C}$ for 15 h. After cooling to room temperature, the crystalline product was filtered and washed with water and acetone, with a yield of 51%. Elemental analysis calculated for $\text{C}_7\text{H}_{11}\text{O}_{15}\text{S}_2\text{Sc}_3$: C, 15.73; H, 2.06; S, 11.99. Found: C, 15.78; H, 1.92; S, 12.08.

$[\text{Sc}(3,5\text{-DSB})(\text{Phen})(\text{H}_2\text{O})](\text{H}_2\text{O})$ (from now on, $(\text{Phen})\text{Sc-MOF}$) was synthesized by addition of $3,5\text{-DSBNa}_2$ (0.052 g, 0.16 mmol) and phenanthroline (0.05 g, 0.32 mmol) to a solution of $\text{Sc}(\text{NO}_3)_3 \cdot 6\text{H}_2\text{O}$ (0.05 g, 0.16 mmol, 6 mL water). The resultant reaction mixture was magnetically stirred at room temperature for 15 min, transferred to a Teflon-lined stainless steel autoclave, and heated at 170 $^{\circ}\text{C}$ for 8 days. After cooling to room temperature, the crystalline product was filtered and washed with water and acetone, with a yield of 83%. Elemental analysis calculated for $\text{C}_{19}\text{H}_{15}\text{N}_2\text{O}_{10}\text{S}_2\text{Sc}$: C, 42.19; H, 2.78; N, 5.18; S, 11.84. Found: C, 42.14; H, 2.48; N, 5.24; S, 11.45.

Single-Crystal Structure Determination. Single-crystal X-ray data for $(\text{O}_2\text{H}_3)\text{Sc-MOF}$ and $(\mu\text{-OH})_3\text{Sc-MOF}$ were collected in a Bruker four-circle kappa diffractometer equipped with a Cu INCOATEC microsource operated at 30 W power (45 kV, 0.60 mA) to generate Cu K α radiation ($\lambda = 1.54178 \text{ \AA}$), and a Bruker APEX II area detector. Data for $(\text{OH})_6\text{Sc-MOF}$ and $(\text{Phen})\text{Sc-MOF}$ were obtained

with a Bruker-Siemens Smart CCD diffractometer equipped with a normal focus, 2.4 kW sealed tube X-ray source (Mo K α radiation = 0.71073 \AA) operating at 50 kV and 30 mA. Data were collected over a hemisphere of the reciprocal space by a combination of three sets of exposures. Each exposure of 20 s covered 0.3 $^{\circ}$ in ω . The unit cell dimensions were determined for a least-squares fit of reflections with $I > 20\sigma$. The structures were solved by direct methods. Compound $(\mu\text{-OH})_3\text{Sc-MOF}$ showed some disorder involving one hydroxyl group; consequently, in the Fourier map, two peaks appeared in the middle distance of Sc1–Sc1 around an inversion center. Each peak was fixed as an oxygen atom and refined with an occupancy factor of 0.5 (O11 and O11A). The final cycles of refinement for both compounds were carried out by full-matrix least-squares analyses with anisotropic thermal parameters for all non-hydrogen atoms. The hydrogen atoms of the aromatic rings were fixed at their calculated positions using distance and angle constraints. The hydrogen atoms from OH, H $_2$ O, and H $_3$ O $_2$ species were located in the corresponding Fourier maps. All calculations were performed using the APEX2 software suite¹⁰ and SMART software¹¹ for data collection, SAINT¹² for data reduction, and SHELXTL to solve and refine the structure.¹³

X-ray Powder Diffraction. X-ray powder diffraction measurements were used to check the purity of the obtained microcrystalline products by comparison of the experimental results with the simulated patterns obtained from single-crystal X-ray diffraction data. The residues for the compounds after TGA were analyzed by X-ray powder diffraction and compared with ICSD patterns reported.

General Procedure for the Cyanosilylation of Aldehyde Substrates. Catalyst (5 mol%) and benzaldehyde (0.74 mmol) were successively placed into a Schlenk flask (volume $\sim 10 \text{ mL}$) in the absence of solvent. A Teflon-coated magnetic stir bar was added, and the reaction was initiated by addition of trimethylsilyl cyanide (TMSCN, 1.1 mmol). The reaction mixture was vigorously stirred (800 rpm) at 40 $^{\circ}\text{C}$ under a N $_2$ atmosphere. The conversion of benzaldehyde and the product yield were followed by gas chromatography (GC) analysis. After the reaction was completed, the catalyst was removed by filtration and centrifugation of the reaction mixture. All products (cyanohydrin trimethylsilyl ethers) were confirmed by comparison of their GC retention times and GC-MS spectra with those of authentic samples. GC analysis was performed using a Konik HRGC 4000B gas chromatograph/mass spectrometer and cross-linked (95%)-dimethyl-(5%)-diphenylpolysiloxane (Teknokroma TRB-SMS) column of 30 m length.

Recycling Experiments. A reuse experiment was carried out for the cyanosilylation of benzaldehyde. The reaction was carried out under the standard conditions. After the reaction was completed, the catalyst was recovered by filtration, washed (ca. 3 mL), and air-dried prior to being reused. The PXRD pattern of the retrieved catalyst was identical to that of the fresh catalyst (Supporting Information Figure S7). The recovered catalyst could be reused for cyanosilylation of benzaldehyde without an appreciable loss of its high catalytic performance. When the cyanosilylation of benzaldehyde was carried out with the recovered catalyst under the standard conditions, cyanohydrin trimethylsilyl ether was obtained in 98% yield.

Computational Details. Plane-wave density functional (PW-DF) calculations were done using the VASP package.¹⁴ The energy was calculated employing the generalized gradient approximation, in particular, the exchange and correlation functional of Perdew and Wang (PW91).¹⁵ The effect of the core electrons on the valence electron density was described by the projector augmented wave (PAW) method.¹⁶ The cutoff for the kinetic energy of the plane waves was set to 415 eV throughout, which after extensive tests proved to ensure a total energy convergence better than 10 $^{-6}$ eV. Geometry optimization was carried out using a gradient-conjugate method. The formation energy (ΔE_{form}) was calculated as the difference between the corresponding energies of the reagents and MOF structures. Total charge representation was performed using VESTA package v.3.¹⁷

■ RESULTS AND DISCUSSION

Effect of Synthesis Conditions. In order to obtain pure phases in the Sc-(3,5-DSB) system, several synthetic experiments

were carried out. It was experimentally observed that both $(\text{O}_2\text{H}_3)_3\text{Sc-MOF}$ and $(\mu\text{-OH})_3\text{Sc-MOF}$ were obtained only when a slight excess of ligand was used, thus establishing the reactants in 1:1 relation (the relation Sc^{III} :ligand in both $(\text{O}_2\text{H}_3)_3\text{Sc-MOF}$ and $(\mu\text{-OH})_3\text{Sc-MOF}$ is 3:2). The effects of pH, temperature, and reaction time were then studied, showing that within pH and temperature ranges of 2.8–3.5 and 200–220 °C, respectively, mixtures of both $(\text{O}_2\text{H}_3)_3\text{Sc-MOF}$ and $(\mu\text{-OH})_3\text{Sc-MOF}$ appear. In order to obtain the two compounds as pure phases, a good number of experiments were carried out with the following results: (i) Up to 170 °C, no reaction takes place. (ii) When temperature increases up to 200 °C, the $(\text{O}_2\text{H}_3)_3\text{Sc-MOF}/(\mu\text{-OH})_3\text{Sc-MOF}$ mixture is present up to 24 h; after this time $(\text{O}_2\text{H}_3)_3\text{Sc-MOF}$ is the only reaction product. (iii) Upon increasing temperature to 220 °C, the amount of $(\mu\text{-OH})_3\text{Sc-MOF}$ in the mixture increases with time up to 3.5 h, but in 4 h $(\text{O}_2\text{H}_3)_3\text{Sc-MOF}$ is isolated as the only reaction product (Supporting Information S4). (iv) Synthesis performed within a 3.5–4 pH range led to a third compound, $(\mu\text{-OH})_6\text{Sc-MOF}$. When pH is higher than 4, only $\text{ScO}(\text{OH})$ is formed (Figure 1).

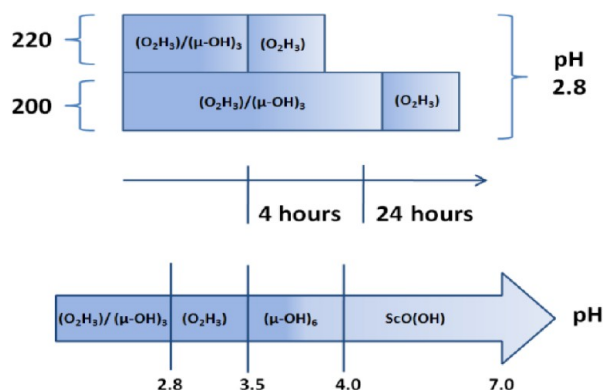


Figure 1. Scanning reaction conditions in the Sc-(3,5-DSB) system ($(\text{O}_2\text{H}_3) = (\text{O}_2\text{H}_3)_3\text{Sc-MOF}$, $(\text{OH}) = (\mu\text{-OH})_3\text{Sc-MOF}$, and $(\mu\text{-OH})_3 = (\mu\text{-OH})_3\text{Sc-MOF}$).

All in all, contrary to what was expected, $(\mu\text{-OH})_3\text{Sc-MOF}$ was only obtained as an intermediate phase mixed with $(\text{O}_2\text{H}_3)_3\text{Sc-MOF}$. The latter can be reached in the indicated pH range under several conditions, since it is the final product of the performed reactions, but the highest yield is obtained at pH 3.5, $T = 220$ °C, and $t = 24$ h. To bring some light to this reaction, theoretical stability calculations were also carried out (see below).

Structural Description. The details of data collection, refinement, and crystallographic data are summarized in Table 1, and ORTEP drawings of the structures are presented in Figure 2.

$(\text{O}_2\text{H}_3)_3\text{Sc-MOF}$ crystallizes in the triclinic space group $P\bar{1}$, and its asymmetric unit is formed by two crystallographically independent ScO_6 hexa-coordinated scandium cations. Sc1 is coordinated to two oxygen atoms of sulfonate groups (O1, O2#), one oxygen atom of carboxylate group (O7), one hydroxyl anion (O9), one water molecule (O11), and one symmetric $[\text{H}_3\text{O}_2]^-$ aqua-hydroxo anion (O10). Sc2, which is located at the $1/2, 1/2, 1/2$ inversion center, coordinates to two oxygen atoms of sulfonate groups (O4, O4#), two oxygen atoms of carboxylate group (O8, O8#), and two hydroxyl anions (O9, O9#) (Figure 2, left).

The ScO_6 primary building units (PBUs) are linked via two μ -hydroxyl bridges to form Sc_3O_{16} trimeric secondary building units (SBUs). These SBUs are connected along the b and c

directions by the η^2, μ_2 -carboxylate and one η^2, μ_2 -anti-syn-sulfonate groups. The other sulfonate group coordinates only to Sc2 ion in an η^1 -anti mode. This arrangement gives rise to a bidimensional structure with the layers perpendicular to the a direction (Scheme 1, Figure 3). In the topological representation, by considering the trimeric SBUs and the ligand as nodal points (Figure 3), a 2D binodal 3,6-connected plane net of the **kfd** type is assigned, with point (Schläfli) symbol $(4^3)^2(4^6.6^6.8^3)$ (TOPOS).¹⁸

The layers are hydrogen-bond-connected via coordinated water molecules and sulfonate oxygen atoms. These interactions give rise to a three-dimensional supramolecular net. For its topological simplification,² only the strongest hydrogen bond that provides dimensionality to the network (interlayer hydrogen bond with a distance $\text{O11-H11A}\cdots\text{O3} = 2.712(3)$ Å) has been taken into account (Figure 4). As a consequence of the new connections, the ligand becomes 4-connected, and the trimeric unit 8-connected. By doing that, the final 3D network is a 4,8-connected net of type fluorite (sqc169) with point (Schläfli) symbol $(4^{12}.6^{12}.8^4)(4^6)^2$.

$(\mu\text{-OH})_3\text{Sc-MOF}$ crystallizes, like $(\text{O}_2\text{H}_3)_3\text{Sc-MOF}$, in the triclinic space group $P\bar{1}$, with two crystallographically independent scandium ions in ScO_6 octahedral arrangement (Figure 2, right). For Sc1, the octahedral environment is formed by oxygen atoms from two hydroxyl anions (O9, O11), two water molecules (O10, O12), one carboxylate group (O8), and one sulfonate group (O4). Sc2, which is located at the inversion center, coordinates to six oxygen atoms from two hydroxyl anions (O9, O9#), two carboxylate (O7, O7#), and two sulfonate groups (O1, O1#). The SBUs in this compound are infinite chains of $\mu\text{-OH}$ sharing a vertex along the $[01-1]$ direction. The carboxylate group in an η^2, μ_2 mode bridges alternatively the polyhedra along the same direction. Joining among SBUs is made along the $[010]$ direction, via η^1, η^1 -anti-anti-sulfonate groups. This arrangement gives rise to a 2D extension of the structure, with the layers perpendicular to the $[100]$ (Figure 5). For the 2D net topological study, the model has been simplified as follows: The chain nodes were placed in the Sc1–Sc2 distance middle points, where the chains are joined by the ligand that acts as a linker. As a result of this simplification, a 2D uninodal 4-connected net of type sql/Shubnikov tetragonal plane net is assigned, with point (Schläfli) symbol $(4^4.6^2)$.

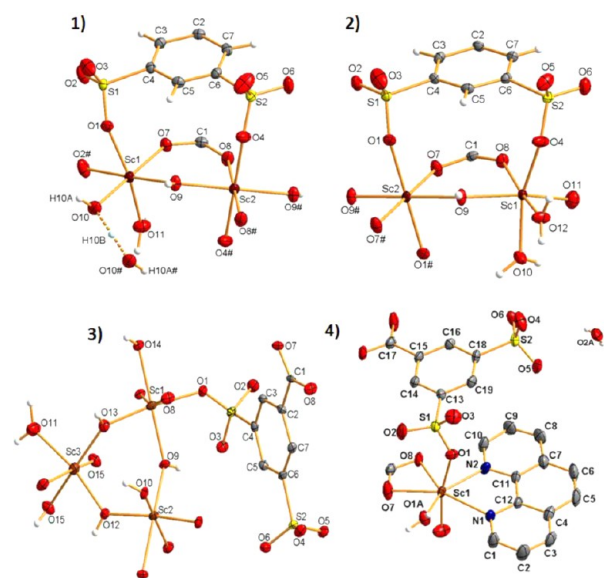
Following the same criteria for simplification used for the other compound (the interlayer hydrogen bond $\text{O9-H9}\cdots\text{O3} = 2.818(4)$ Å), the final 3D network resulted in a 6-connected uninodal net with point (Schläfli) symbol $(4^{12}.6^3)$ and topological type pcu α -Po primitive cubic (Figure 6).

$(\mu\text{-OH})_6\text{Sc-MOF}$ has a 3D network and consists of three crystallographically independent scandium ions in ScO_6 octahedral arrangement. These three octahedra share a vertex via $\mu\text{-OH}$ anions to give $[\text{Sc}_3(\mu\text{-OH})_3]^{6+}$ clusters. Each of these three polyhedra also shares edges $[\text{Sc}-(\mu\text{-OH})_2\text{-Sc}]$ with its centro-symmetric one, giving rise to six-polyhedra SBUs, whose linkage generates nine ring containing hydroxo-scandate inorganic layers (**9R-IL**) parallel to the (110) plane. The ligand coordinates through the carboxylate group in an η^2, μ_2 mode, and through the sulfonate groups in an η^1 -anti mode and an η^2, μ_2 -anti-anti mode. The latter, joining the inorganic layers along the $[100]$ direction, acts as pillar that gives rise to the 3D net.

This structure was topologically analyzed as follows: **9R-IL** was simplified by setting the nodal points at the center of the SBUs (Figure 7). This simplification resulted in a 3-connected

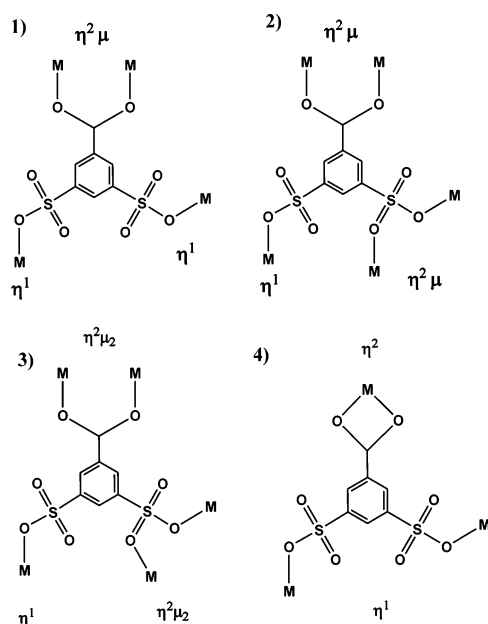
Table 1. Crystal and Refinement Data for the Compounds (O₂H₃)Sc-MOF, (μ-OH)₃Sc-MOF, (μ-OH)₆Sc-MOF, and (Phen)Sc-MOF^a

	(O ₂ H ₃)Sc-MOF	(μ-OH) ₃ Sc-MOF	(μ-OH) ₆ Sc-MOF	(Phen)Sc-MOF
empirical formula	C ₁₄ H ₁₅ O ₂₂ S ₄ Sc ₃	C ₁₄ H ₁₇ O ₂₃ S ₄ Sc ₃	C ₇ H ₁₁ O ₁₅ S ₂ Sc ₃	C ₁₅ H ₁₄ N ₂ O ₉ S ₂ Sc
FW	798.42	816.44	794.57	540.43
T (K)	298(2)	298(2)	298(2)	298(2)
wavelength (Å)	1.54178	0.71073	1.54178	0.71073
crystal system	triclinic	triclinic	triclinic	monoclinic
space group	P $\bar{1}$	P $\bar{1}$	P $\bar{1}$	P2/c
unit cell dimensions				
<i>a</i> (Å)	7.5624(5)	7.5148(1)	7.7832(2)	15.1476(2)
<i>b</i> (Å)	9.2132(6)	9.5270(2)	9.7208(2)	9.9236(10)
<i>c</i> (Å)	9.7011(6)	10.2296(2)	11.6659(3)	14.1593(2)
α (°)	100.366(3)	69.198(2)	65.874(1)	90
β (°)	99.102(3)	85.365(3)	80.743(1)	102.873(2)
γ (°)	104.809(3)	82.458(3)	84.443(1)	90
<i>V</i> (Å ³)	627.81(7)	678.25(2)	794.57(3)	2074.9(4)
<i>Z</i>	1	1	2	4
ρ (Mg/m ³)	2.112	2.001	2.233	1.73
<i>F</i> (000)	401.0	411.0	536	1228
θ range (°)	4.74–63.70	2.13–25.02	4.19–63.75	1.38–26.37
reflns collected/unique	2739/1949	5083/2338	11182/2486	16718/4242
completeness (%)	94.4	97.3	95.0	99.8
data/restraint/parameters	1949/0/208	2338/0/220	2486/0/245	4242/0/357
goodness-of-fit, <i>F</i> ²	1.063	1.073	1.056	1.047
<i>R</i> 1 [<i>I</i> > 2σ(<i>I</i>)]	0.0252	0.0348	0.0337	0.0689
<i>wR</i> 2 [<i>I</i> > 2σ(<i>I</i>)]	0.0715	0.0844	0.0954	0.1571
<i>R</i> 1 (all data)	0.0261	0.0441	0.0355	0.1258
<i>wR</i> 2 (all data)	0.0721	0.878	0.0967	0.2011
largest diff	0.343, −0.392	0.433, −0.347	0.589, −1.050	0.541, −0.516

^aAbsorption correction: semiempirical from equivalents in all cases. Refinement method: full-matrix least-squares on *F*² in all cases.**Figure 2.** ORTEP drawings of (1) (O₂H₃)Sc-MOF, (2) (μ-OH)₃Sc-MOF, (3) (μ-OH)₆Sc-MOF, and (4) (Phen)Sc-MOF. Ellipsoids are displayed at the 50% probability level.

uninodal net of type hcb (Shubnikov hexagonal plane) with (Schlafli) symbol (6³).

In a second stage, the role of the ligand in the 3D network was analyzed. By observing the ligand, we see that one sulfonate and the carboxylate groups are coordinated to the same inorganic layer and do not contribute to the network dimensionality. It is

Scheme 1. Representation of Coordination Modes for 3,5-DSB Ligand in (1) (μ-OH)₃Sc-MOF, (2) (O₂H₃)Sc-MOF, (3) (μ-OH)₆Sc-MOF, and (4) (Phen)Sc-MOF

the other sulfonate group, which acts as a bridge between the two 9R-ILs (Figure 8), that is responsible for the resulting bnn hexagonal net, with a 5-connected node and (Schlafli) symbol (4⁶.6⁴).

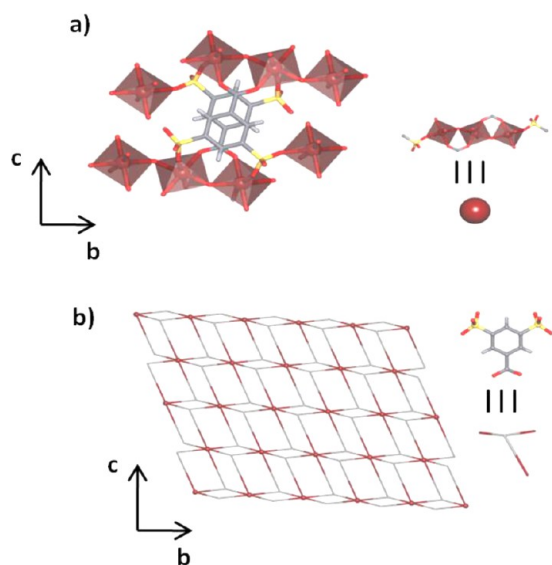


Figure 3. $(\text{O}_2\text{H}_3)\text{Sc-MOF}$: (a) polyhedral representation of the net and SBU and (b) the *kgd* topological net.

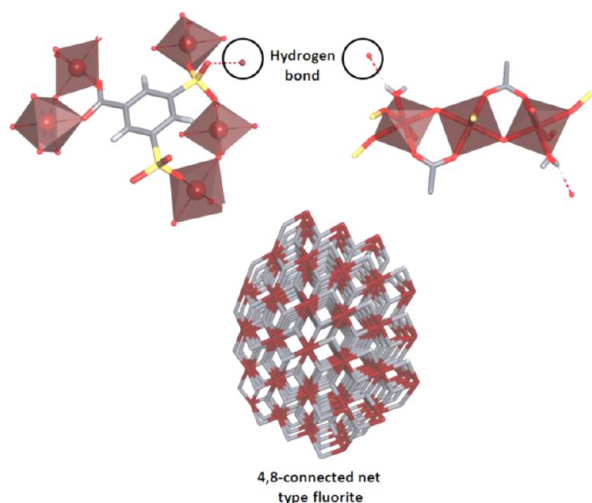


Figure 4. $(\text{O}_2\text{H}_3)\text{Sc-MOF}$ hydrogen bond representation and simplification of the 3D supramolecular net.

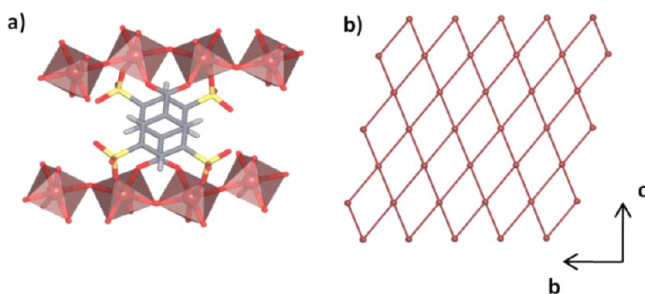


Figure 5. (a) Representation of the polyhedrons in the SBUs. (b) Representation of the simplified net of type *sql*/Shubnikov tetragonal plane for $(\mu\text{-OH})_3\text{Sc-MOF}$.

For structural and catalytic comparative purposes, $(\text{Phen})\text{Sc-MOF}$, in which the Phen ligand blocks two of the Sc coordination sites and in whose formula $[\text{Sc}(3,5\text{-DSB})(\text{Phen})(\text{H}_2\text{O})](\text{H}_2\text{O})$ appears neither OH group nor H_3O_2^- anion, was also obtained. It crystallizes in the monoclinic space group $P2_1/c$. The Sc^{III} is

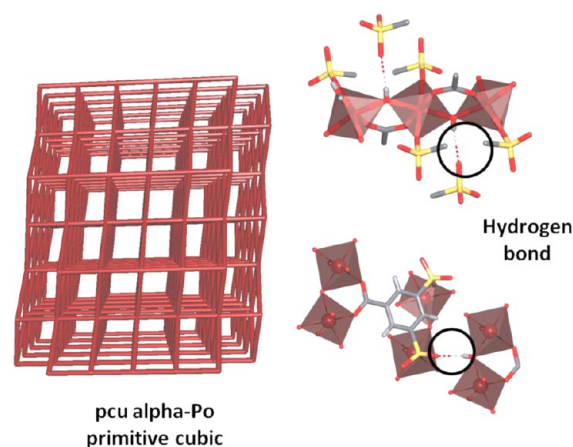


Figure 6. Hydrogen bond representation and simplification of the supramolecular net for $(\mu\text{-OH})_3\text{Sc-MOF}$.

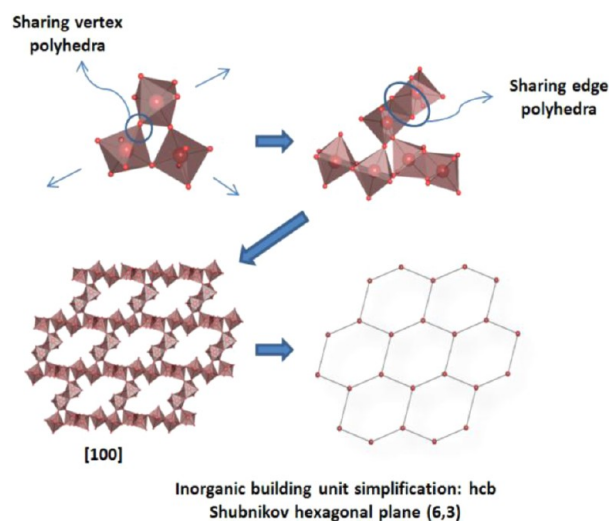


Figure 7. Representation of the formation of the inorganic building unit for $(\mu\text{-OH})_6\text{Sc-MOF}$.

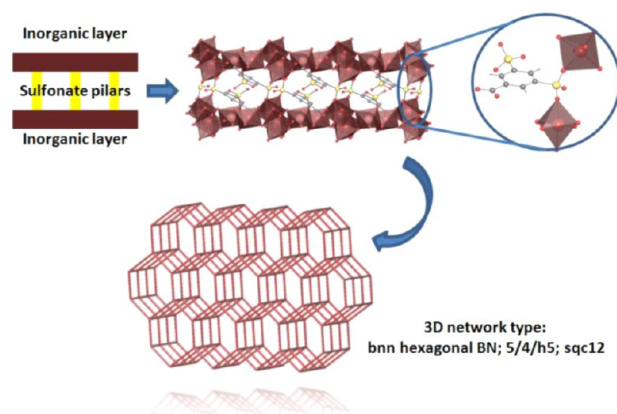


Figure 8. Representation of the 3D net and simplification for $(\mu_2\text{-OH})\text{Sc-MOF}$.

hepta-coordinated to four ligand oxygen atoms, one water molecule, and two phenanthroline nitrogen atoms in a (ScO_3N_2) polyhedron. The DSB ligand acts as an η^2 chelate mode via carboxylate group, and an $\eta^1\text{-anti}$ -mode via both sulfonate groups. As two of the Sc^{III} coordination sites are blocked by the

chelate phenanthroline ligand, the 3,5-DSB anion acts as a tritopic ligand, linking three different metallic centers. This arrangement gives rise to polymeric ladder-like chains along the [001] direction, which are linked to each other through hydrogen bonds along the [010] direction (distance $\text{O}\cdots\text{H}\cdots\text{O} = 2.725(6)\text{\AA}$), forming layers parallel to the (011) plane. Among them (direction [100]), π - π stacking and nonconventional $\text{C}\cdots\text{H}\cdots\text{O}$ interactions are observed.

π - π stacking interactions appear among the phenanthroline rings, with distances of $3.5944(4)$ and $3.7596(4)$ \AA and dihedral angle of 1.39° . The $\text{C}\cdots\text{H}\cdots\text{O}$ interactions are generated through one of the phenanthroline $\text{C}\cdots\text{H}$ and one oxygen of the sulfonate group. The distance and angle ($\text{C6}\cdots\text{H6}\cdots\text{O3}$) are $3.326(9)$ \AA and $166.13(7.77)^\circ$, respectively. This arrangement creates a 3D supramolecular net (Figure 9).

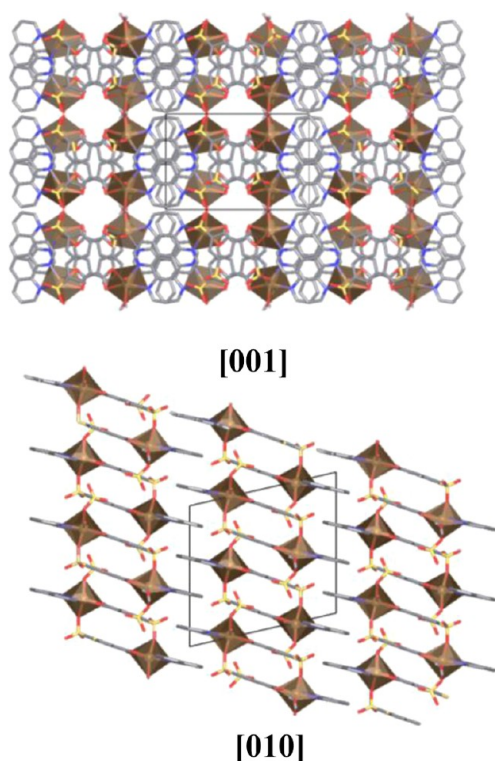


Figure 9. View of the crystal packing along the [001] and [010] directions for (Phen)Sc-MOF.

From a topological point of view, by considering only the covalent net, the 3,5-DSB ligand acts as a linker among the trivalent 3-connected cations and gives rise to a uninodal 1D SP 1-periodic net $(4,4)(0,2)$ (Figure 10), with point (Schläfli) symbol $(4^2.6)^{18}$. On the other hand, when including the hydrogen bonds that join the double chains to form layers (Figure 10), the additional bond generates a 4-connected node, allowing the formation of the SP 2-periodic net $(6,3)\text{Ia}$, with point (Schläfli) symbol $(4^3.6^3)^{18}$.

Hydrogen Oxide $\text{M}\cdots\text{H}_3\text{O}_2\cdots\text{M}$ Bridging Ligand. $(\text{O}_2\text{H}_3)\text{Sc-MOF}$ is the first example of the $\mu\text{-H}_3\text{O}_2^-$ bridging ligand in a MOF material. The presence of the $[\text{H}_3\text{O}_2]^-$ anion is clear, on the basis of the crystallographic data. The bridging hydrogen atom was located from the difference Fourier map (H10B) in an inversion center at $1/2, 0, 1/2$, with distances $\text{O10}\cdots\text{H10B} = 1.222(2)$ \AA and $\text{O10}\cdots\text{O10B} = 2.445(3)$ \AA (Figure 2). In order to verify the symmetry of the $[\text{H}_3\text{O}_2]^-$ bonds, the inversion

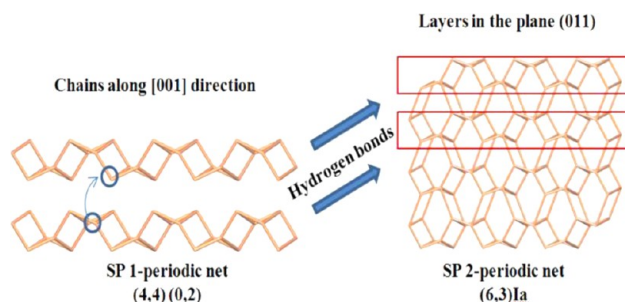


Figure 10. Schematic representation of 1D polymeric chain in "ladder" form (simplification without hydrogen bonds) and the formation of layers by hydrogen bonding for (Phen)Sc-MOF.

center was avoided, and the structure was refined in the space group $P1$. The shared proton was again located in coordinates corresponding to similar distance values: $\text{O10A}\cdots\text{O10B} = 2.449(2)$ \AA , $\text{O10A}\cdots\text{H10B} = 1.23(1)$ \AA , and $\text{O10B}\cdots\text{H10B} = 1.22(1)$ \AA . Although more accurate data on the location of the central H atom could be obtained by neutron diffraction, the present X-ray data together with the characteristic $\text{M}\cdots\text{M}$ intermetallic distance around 5 \AA (in our case $\text{Sc1}\cdots\text{Sc1} = 5.4158(7)$ \AA) completely agree with theoretical and experimental works on this anion reported in transition metal dimeric complexes,^{9c} and support the existence of the (O_2H_3) bridge in the present MOF.

Although we cannot properly think of dimers in an extended net, by making abstraction of the two Sc complex fragments involved in the $\mu\text{-O}_2\text{H}_3$ formation, it can be seen that in $(\text{OH})_3\text{Sc-MOF}$ each of these two Sc cations bears two *cis*-coordinated water molecules (Figure 11, top), forming faced $\text{Sc}(\mu\text{-OH})(\text{H}_2\text{O})_2$ halves, quite similar to the aqua-hydroxo double salt precursors. In these salts, ololation^{9a-d} reactions take place to give the thermodynamically stable double μ -hydroxo dimer: $[\text{L}_x\text{M}(\text{H}_3\text{O}_2)\text{ML}_x] \rightarrow [\text{L}_x\text{M}(\text{OH})_2\text{ML}_x] + \text{H}_2\text{O}$. On the basis of our synthetic procedure experience and theoretical calculation, it seems that in the $(\text{O}_2\text{H}_3)\text{-Sc} \leftrightarrow (\text{OH})\text{-Sc}$ equilibrium the MOF formation reaction goes in the opposite direction, $[\text{Sc}_3(3,5\text{-DSB})_2(\mu\text{-OH})_3(\text{H}_2\text{O})_4]_2 \rightarrow [\text{Sc}_3(3,5\text{-DSB})_2(\mu\text{-O}_2\text{H}_3)(\mu\text{-OH})_2(\text{H}_2\text{O})_2] + \text{H}_2\text{O}$, since the hydroxo species is much less thermodynamically stable than the aqua-hydroxo one.

The loss of one water molecule from each double $[\text{Sc}(\mu\text{-OH})(\text{H}_2\text{O})_2]_2$ fragment to give $[\text{Sc}_2(\mu\text{-OH})_2(\text{H}_2\text{O})_3]$, and H_3O_2 bridge formation between one water molecule and one $\mu\text{-OH}$ anion, yield in the thermodynamically very stable $[\text{Sc}_3(3,5\text{-DSB})_2(\mu\text{-O}_2\text{H}_3)(\mu\text{-OH})_2(\text{H}_2\text{O})_2]$ MOF (Figure 7). The vacant positions in the involved Sc coordination sphere variations are occupied by oxygen atoms of those sulfonate groups that modify their coordination mode from η^1 to η^2, μ (Figure 11). Structurally speaking, the distance $\text{Sc}\cdots\text{Sc}$, $3.8448(7)$ \AA in $(\mu\text{-OH})_3\text{Sc-MOF}$, expands to $5.4158(7)$ \AA in $(\text{O}_2\text{H}_3)\text{Sc-MOF}$. Among other reasons that could justify this experimental fact, probably the nature of the MOF and the versatile coordination of the 3,5-DSB ligand are what stabilize the (O_2H_3) bridge.

IR Spectra. Given the lack of IR data for MOFs containing $\text{M}\cdots\text{H}_3\text{O}_2\cdots\text{M}$ bonds, and with the aim of comparing both $(\text{O}_2\text{H}_3)\text{Sc-MOF}$ and $(\mu\text{-OH})_3\text{Sc-MOF}$ spectra, a few crystals of the latter (precursor phase) were hand-selected, and the IR spectra of both MOFs were recorded (Figure 12). The bands in the region of $\sim 1020\text{--}1140$ cm^{-1} are related with the coordination of the sulfonate group. In this region we find four

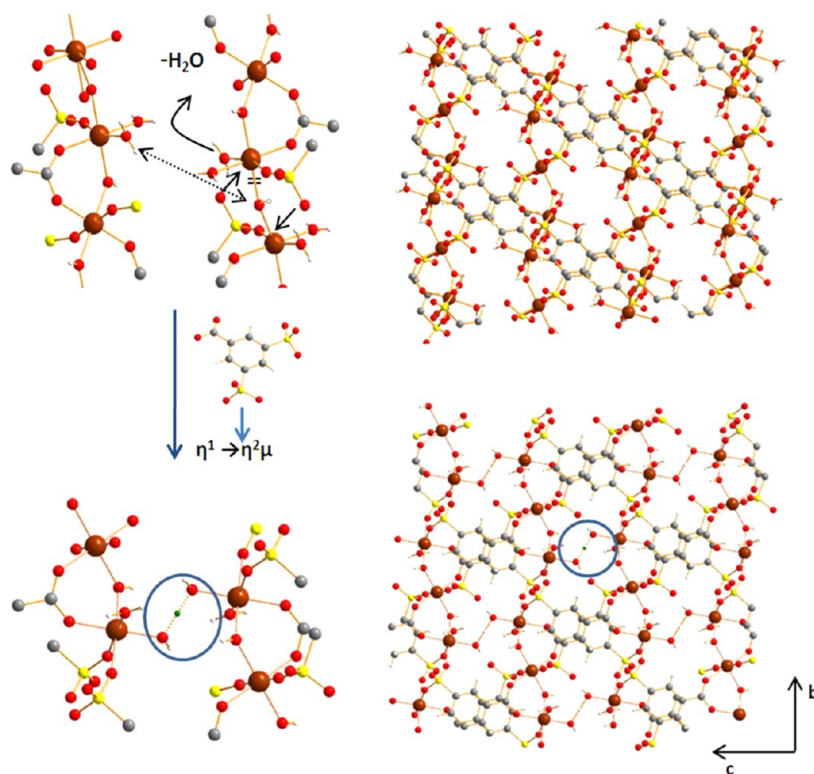


Figure 11. Hydrogen oxide $M-H_3O_2-M$ bridging ligand formation. Structural changes from (top) $(\mu-OH)_3Sc-MOF$ to (bottom) $(O_2H_3)Sc-MOF$.

bands characteristic of a bridged bidentate coordination mode ($\eta^2\mu_2$) and three bands for a unidentate mode (η^1) that correspond with $(O_2H_3)Sc-MOF$ and $(\mu-OH)_3Sc-MOF$, respectively (Figure 12a).¹⁹ In the region between ~ 1600 and 1670 cm^{-1} , we observe the HO bending vibration. For $(O_2H_3)Sc-MOF$ it is observed that the bands are slightly displaced to the high-energy region with respect to $(\mu-OH)_3Sc-MOF$, and the band situated at $\sim 1625\text{ cm}^{-1}$ presents a decrease in intensity, indicating symmetrization in the central OHO vibration of the $O_2H_3^-$ species (Figure 12b).²⁰ Two bands that appear in the region $\sim 3150\text{--}3420\text{ cm}^{-1}$ are associated with the O–H stretching bands of the hydroxide anion. These bands are also associated with the overtones of the mixed ionic H-bonded OH stretch/H–O–H bending modes (Figure 12c).²¹ The bands in the region of $\sim 420\text{--}470\text{ cm}^{-1}$ are assigned to M–O vibrations. IR spectra for $(\mu-OH)_6Sc-MOF$ and $(Phen)Sc-MOF$ can be found in Supporting Information S2.

Thermal Study. The thermogram for $(O_2H_3)Sc-MOF$ shows a mass loss corresponding to two water molecules, one hydroxyl group, and the aquo-hydroxo species around $280\text{ }^\circ\text{C}$ (calculated 9.02%, found 9.9%). Decomposition of the organic ligand begins at $\sim 520\text{ }^\circ\text{C}$. At higher temperature, loss of the SO_3 molecule is observed (calculated 7.8%, found 7.6%), and the compound decomposes to give finally Sc_2O_3 .²²

TGA for $(Phen)Sc-MOF$ shows a loss of mass around $120\text{ }^\circ\text{C}$, which corresponds with loss of the coordinated and free water molecules (calculated 6.7%, found 7.1%). The total decomposition of the framework begins at $\sim 470\text{ }^\circ\text{C}$, where we observe the loss of the organic ligands (calculated 80.49%, found 80.8%) and the formation of Sc_2O_3 as a decomposition product.

The decomposition profile of $(\mu-OH)_6Sc-MOF$ is similar to that of the above compound, where the mass loss corresponding to loss of the water molecule and hydroxyl group is observed around $250\text{ }^\circ\text{C}$, followed by decomposition of the ligand at ~ 520

$^\circ\text{C}$ and finally by the total decomposition to Sc_2O_3 .²² The decomposition product was confirmed by comparison of its PXRD pattern with that reported for Sc_2O_3 .²³

Theoretical Stability Studies. In recent years PW-DF calculations have been used as a characterization tool to study the thermodynamical stability of crystal phases and its effect on the crystallization process in the MOF syntheses.²⁴ The great potential of this type of calculations is known in determination of the electronic properties of different kinds of compounds. Theoretical calculations of the apparent energies of formation were carried out using the VASP package (see Computational Details). Geometry optimization was done using the experimental structures obtained by X-ray diffraction and always converged to a stable structure, even though no symmetry constraints were imposed in this case.

With the purpose of elucidating, from an energetic point of view, the aqua-hydroxo and the hydroxyl $Sc-MOF$ formation, we performed theoretical calculations. In addition, a study of the $(O_2H_3)Sc-MOF$ electronic structure was also carried out to determine the nature of the O---H---O bond.

Although the $(\mu-OH)_6Sc-MOF$ compound is obtained at higher pH than the other two compounds, and thus, it is not subject to the aqua-hydroxo and hydroxyl equilibrium, this third compound was also included in the calculations for comparative purposes only.

Taking into account the results of the calculated formation energies (Figure 13), it can be concluded that the $(O_2H_3)Sc-MOF$ presents a lower formation energy (ΔE_{For}) than the $(\mu-OH)_3Sc-MOF$. This fact and the experimental results indicate that, under these synthesis conditions, the formation of the most stable phase is favored, and thus this is a thermodynamically governed process.

For short times and $\text{pH} < 2.8$, $(\mu-OH)_3Sc-MOF$ and $(O_2H_3)Sc-MOF$ coexist. When temperature increases, $(\mu-$

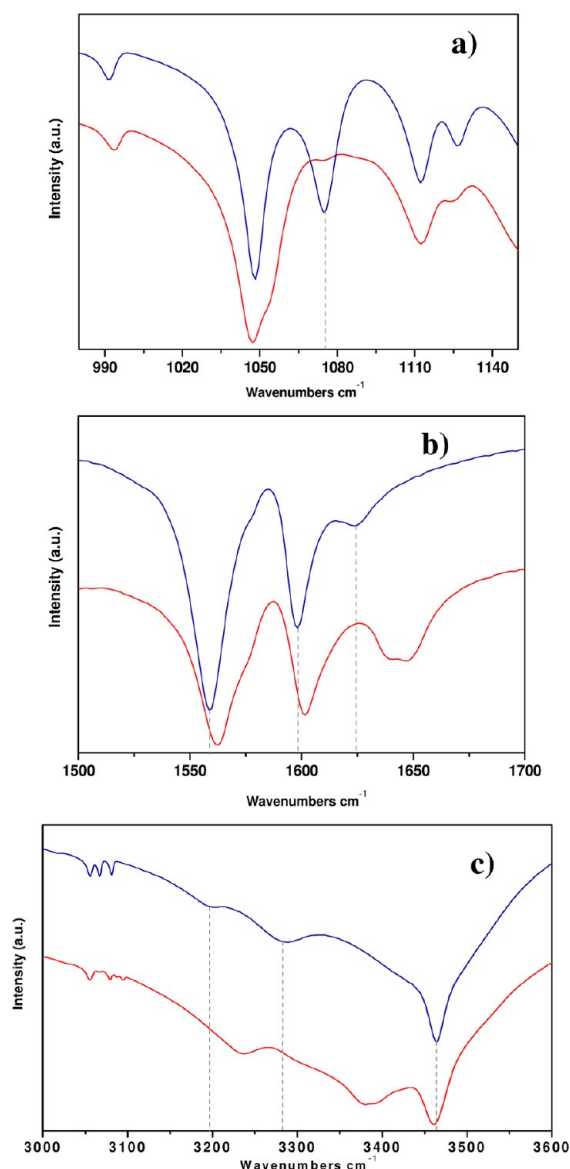


Figure 12. IR profiles for $(\text{O}_2\text{H}_3)\text{Sc-MOF}$ (blue) and $(\mu\text{-OH})_3\text{Sc-MOF}$ (red): (a) S–O for η^1 - and η^2,μ -sulfonate groups, (b) HOH bending vibration, and (c) OH stretch/H–O–H bending modes.

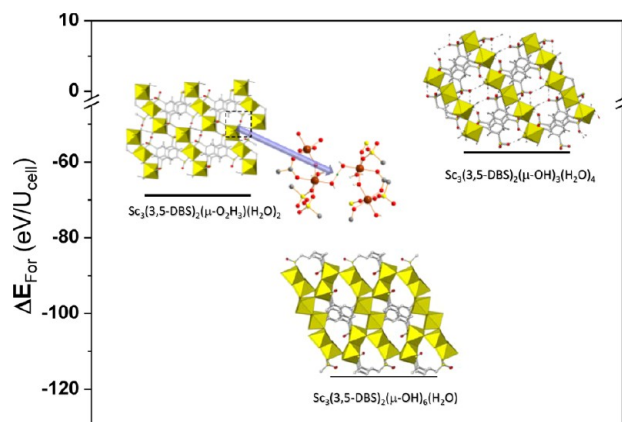


Figure 13. Calculated formation energies ($\Delta E_{\text{Formation}}$) for $(\text{O}_2\text{H}_3)\text{Sc-MOF}$, $(\mu\text{-OH})_3\text{Sc-MOF}$, and $(\mu\text{-OH})_6\text{Sc-MOF}$.

$(\text{OH})_3\text{Sc-MOF}$ appears in a low amount, always as a reaction secondary phase, and reverts with time to the $(\text{O}_2\text{H}_3)\text{Sc-MOF}$ in all cases. This seems to indicate that, in a first stage (at 200 or 220 °C), a kinetic process drives the $(\mu\text{-OH})_3\text{Sc-MOF}$ formation, and then the following loss of a water molecule leads to the formation of the thermodynamically favorable $(\text{O}_2\text{H}_3)\text{Sc-MOF}$. As expected, $(\mu\text{-OH})_6\text{Sc-MOF}$, more condensed 3D structure that appears at higher pH, is the thermodynamically most stable phase.

On the other hand, PW-DF for $(\text{O}_2\text{H}_3)\text{Sc-MOF}$ corroborates the H_3O_2^- species formation. The study of the electronic properties of the OH groups of H_3O_2^- shows that the total charge of oxygen atoms (5.213) is slightly higher than in the case of other hydroxyl groups (5.187), while the H atom that acts as a bridge possesses a lower total charge (0.564) than other hydrogen atoms in OH groups (0.704). In Figure 14, a section of the isosurface total charge is represented for the H_3O_2 molecule, in 2D and 3D views. This picture shows the charge transfer between H_{bridge} and oxygen atoms.

Catalysis. Cyanosilylation reaction provides a convenient route to cyanohydrins, which are key derivatives in the synthesis of fine chemicals and pharmaceuticals.²⁵

This work presents the use of environmentally friendly conditions to study the Lewis acid catalytic activity of the $(\text{O}_2\text{H}_3)\text{Sc-MOF}$, $(\mu\text{-OH})_6\text{Sc-MOF}$, and $(\text{Phen})\text{Sc-MOF}$ compounds. To understand their catalytic properties and to optimize the heterogeneous reaction conditions, they were tested in cyanosilylation reactions. Different reaction conditions were tested (temperature, solvents, % TMSCN, % catalyst), and it was observed that at 40 °C, with 5 mol% of catalyst and ethanol as solvent, the trimethylsilyl benzoate was the main product of reaction (63%, 7 h) for $(\text{O}_2\text{H}_3)\text{Sc-MOF}$. However, when the reaction was performed under an inert atmosphere and in the absence of solvent, we found that $(\text{O}_2\text{H}_3)\text{Sc-MOF}$, $(\mu\text{-OH})_6\text{Sc-MOF}$, and $(\text{Phen})\text{Sc-MOF}$ showed good activity for the cyanosilylation of benzaldehyde, with turnover frequency values of 2.5, 1.8, and 2.1 h^{-1} , respectively. Figure 15 shows the kinetic profile for benzaldehyde. These results show that $(\text{O}_2\text{H}_3)\text{Sc-MOF}$ has a relatively higher activity; thus, it is used for study of the substrate's influence on the catalyst reactivity. Table 2 shows the obtained results. Heptanaldehyde (linear aldehyde) gives the best activity in the cyanosilylation reaction. When using toluene aldehyde, the kinetic profile follows the same trend (Figure 16). Such catalytic behavior is comparable to the best prior results for MOFs,²⁶ and the $(\text{O}_2\text{H}_3)\text{Sc-MOF}$ activity is higher than those of other Sc-MOFs (with CH_2Cl_2 as solvent)^{3e} reported previously.

Catalysts could be easily isolated from the reaction suspension by simple filtration (Supporting Information S7). To demonstrate their recyclability, successive reactions were performed, showing that the activity of the recovered catalyst does not decrease after four cycles at least. Analyses of the reused catalysts, separated from the reaction media, showed that the overall catalyst structure was largely maintained (Figure 17).

It seems quite plausible that the reaction goes, in the three compounds, via displacement of the labile water by the aldehyde before its activation and reaction. This generates a Lewis acid vacancy able to promote the activation of the carbonyl and the cyano addition.²⁷

CONCLUSIONS

$(\text{O}_2\text{H}_3)\text{Sc-MOF}$ is the first example of a MOF material that contains the $\mu\text{-H}_3\text{O}_2^-$ bridging ligand. Structurally speaking,

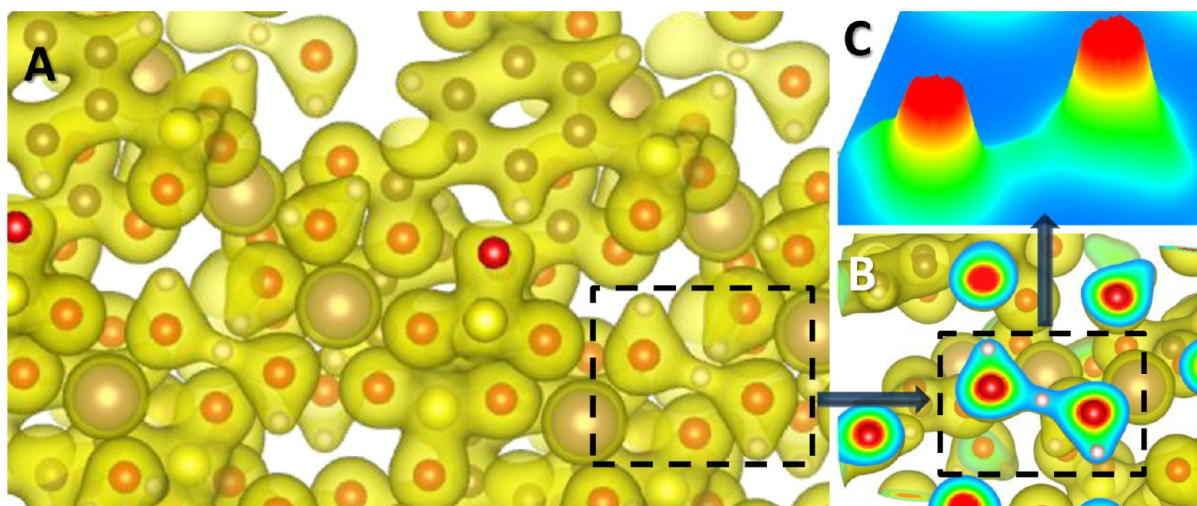


Figure 14. Schematic representation of the total charge for $(\text{O}_2\text{H}_3)\text{Sc-MOF}$: (A) isosurface representation; (B) isosurface section in the plane $(1.224, 3.808, -1)$ containing $\text{OH}\cdots\text{H}-\text{OH}$ atoms, showing the electronic charge transfer H_{bridge} and the nearest O atoms; and (C) bird's-eye view of the total charge around H_3O_2 .

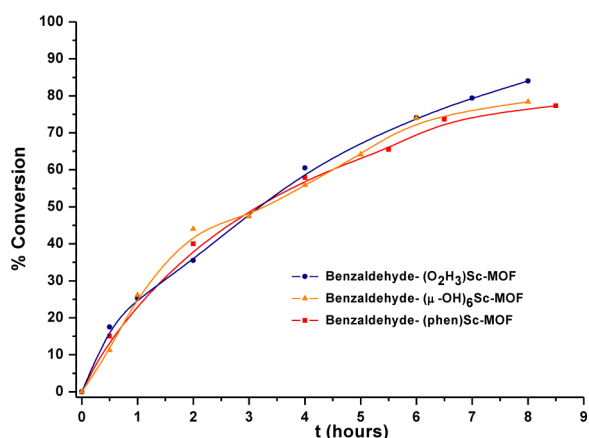


Figure 15. Kinetic profile for the cyanosilylation reaction catalyzed by $(\text{O}_2\text{H}_3)\text{Sc-MOF}$, $(\mu\text{-OH})_6\text{Sc-MOF}$, and $(\text{Phen})\text{Sc-MOF}$.

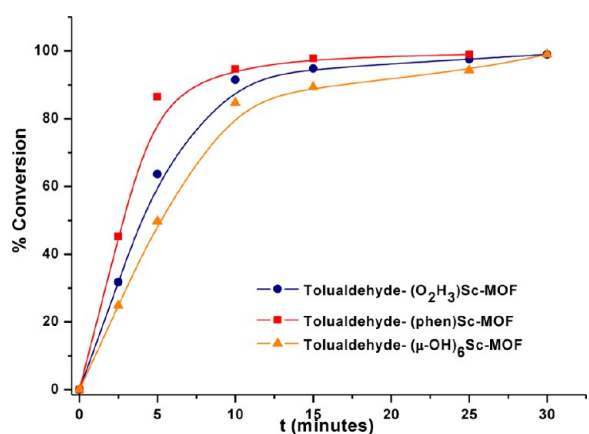
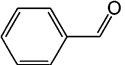
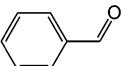
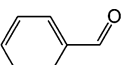
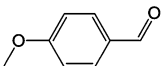
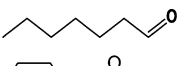
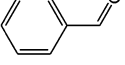
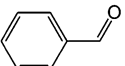


Figure 16. Kinetic profile for the cyanosilylation of *p*-tolualdehyde with $(\text{O}_2\text{H}_3)\text{Sc-MOF}$, $(\mu\text{-OH})_6\text{Sc-MOF}$, and $(\text{Phen})\text{Sc-MOF}$.

besides the clear localization in the Fourier difference map of the bridging H atom, the increase of the Sc–Sc distance from 3.8448(7) Å in $(\mu\text{-OH})_3\text{Sc-MOF}$ to 5.4158(7) Å in $(\text{O}_2\text{H}_3)\text{Sc-MOF}$ evidences the formation of the $(\text{O}_2\text{H}_3)^-$ bridging species.

Table 2. Comparison of the Catalytic Activity for $(\text{O}_2\text{H}_3)\text{Sc-MOF}$, $(\mu\text{-OH})_6\text{Sc-MOF}$, and $(\text{Phen})\text{Sc-MOF}$: Aldehyde Cyanosilylation Reaction Performed with Different Substrates by $(\text{O}_2\text{H}_3)\text{Sc-MOF}$

Compound	Substrate	TOF		
		Time	Yield (%) ^[a]	(h ⁻¹) ^[b]
$(\text{O}_2\text{H}_3)\text{Sc-MOF}$		8 h	84	2.5
$(\mu\text{-OH})_6\text{Sc-MOF}$		8.5 h	77.3	1.8
$(\text{Phen})\text{Sc-MOF}$		7 h	55	2.1
$(\text{O}_2\text{H}_3)\text{Sc-MOF}$		3 h	90	18.5
$(\text{O}_2\text{H}_3)\text{Sc-MOF}$		2 h	100	14.5
$\text{Sc-MOF}^{[c]}$		12 h	90	n.d.
Blank ^[d]		8 h	35	-

^aYield determined by GC-MS. ^bTOF: %Conv/(mmol of substrate / mmol cat. h). ^cReference 2e. ^dReaction performed with benzaldehyde + trimethylsilyl cyanide, 40 °C (blank).

The role that the synthesis conditions play in the formation of each phase has been studied and complemented with theoretical calculations. Taking into account both the synthetic results and the relative formation energies for the compounds that coexist under certain hydrothermal conditions, the thermodynamic or kinetic control of the reaction has been established. $(\mu\text{-OH})_3\text{Sc-MOF}$ is the precursor and less stable phase. When reaction time or temperature increases, $(\text{O}_2\text{H}_3)\text{Sc-MOF}$, the most stable phase, appears, this process being thus thermodynamically controlled. As expected, $(\mu\text{-OH})_6\text{Sc-MOF}$, with a more

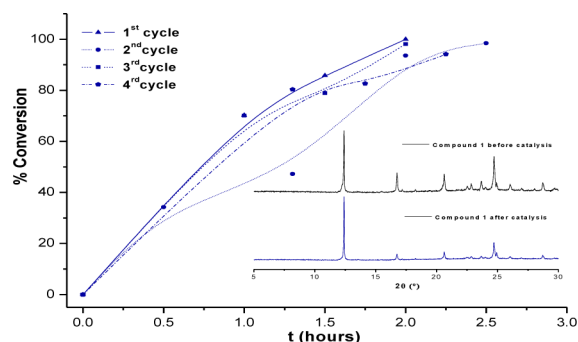


Figure 17. Kinetic profile for the cyanosilylation reaction catalyzed by $(\text{O}_2\text{H}_3)\text{Sc-MOF}$ in four cycles, and the X-ray powder patterns before and after the catalysis.

condensed 3D structure, that appears at higher pH is the thermodynamically most stable phase.

In addition, a theoretical PW-DF study of the $(\text{O}_2\text{H}_3)\text{Sc-MOF}$ electronic structure corroborates the H_3O_2 species formation. Considering structural and topological features of both the uninodal 4-connected sql $(\mu\text{-OH})_3\text{Sc-MOF}$ and the binodal 3,6-connected kgd $(\text{O}_2\text{H}_3)\text{Sc-MOF}$ 2D nets, it can be concluded that hydrogen bonds govern the 3D supramolecular net formations, achieving 6-connected uninodal pcu $\alpha\text{-Po}$ and 4,8-connected net of type fluorite for $(\mu\text{-OH})_3\text{Sc-MOF}$ and $(\text{O}_2\text{H}_3)\text{Sc-MOF}$, respectively.

$(\text{O}_2\text{H}_3)\text{Sc-MOF}$, $(\mu\text{-OH})_3\text{Sc-MOF}$, and $(\text{Phen})\text{Sc-MOF}$ are active as heterogeneous catalysts toward cyanosilylation reactions. The kinetics of the reaction (similar for the three catalysts) mainly depends on the nature of the substrate and the amount of acid sites probably formed via displacement of the labile water by the aldehyde before activation and reaction. The catalytically active species is able to polarize the carbonyl group, making the nucleophilic addition easier.

It is worth to remark that the stabilization of this species in a steady MOF material opens a new field of study of new properties including protonic conductivity (in our $(\text{O}_2\text{H}_3)\text{Sc-MOF}$, the proton is situated in the middle of the channels), water splitting, or even, in enzymatic reactions, hydrogen atom transfer via H_3O_2 bridging.

■ ASSOCIATED CONTENT

■ Supporting Information

Selected bond lengths and angles, FT-IR spectroscopy of $(\text{O}_2\text{H}_3)\text{Sc-MOF}$, experimental and simulated PXRD patterns, TGA, X-ray powder patterns after TGA, and X-ray powder patterns after catalytic studies for $(\text{O}_2\text{H}_3)\text{Sc-MOF}$, $(\mu\text{-OH})_3\text{Sc-MOF}$, and $(\text{Phen})\text{Sc-MOF}$. This material is available free of charge via the Internet at <http://pubs.acs.org>. CCDC reference numbers 865076, 865077, 865078, and 865079 contain crystallographic data for this paper. These data can be obtained free from the Cambridge Crystallographic Data Centre via www.ccdc.cam.ac.uk/data_request/cif.

■ AUTHOR INFORMATION

Corresponding Author

amongue@icmm.csic.es

Notes

The authors declare no competing financial interest.

■ ACKNOWLEDGMENTS

R.F.D. acknowledges a FPI scholarship from Spanish Ministry of Economy and Competitiveness (MINECO), and Fondo Social Europeo from the EU. V.A.P.O. acknowledges financial support from the MCYT in the Ramon y Cajal Program and ENE2009-09432. Computational time has been provided by the Centre de Supercomputació de Catalunya (CESCA) and the Centro de Supercomputación de Galicia (CESGA). This work has been supported by the Spanish MCYT Project MAT2010-17571, MAT2011-29020-C02-02, FAMA S2009/MAT-1756 Comunidad Autónoma de Madrid, and Consolider-Ingenio CSD2006-2001.

■ REFERENCES

- (1) (a) Cotton, S. A. *Lanthanide and Actinide Chemistry*; John Wiley & Sons: Uppington, Rutland, UK, 2006. (b) Chu, Y.; Liu, X.; Li, W.; Hu, X.; Lin, L.; Feng, X. *Chem. Sci.* **2012**, *3*, 1996. (c) Iimura, S.; Manabe, K.; Kobayashi, S. *Tetrahedron* **2004**, *60*, 7673. (d) Nishiura, M.; Hou, Z. *Nat. Chem.* **2010**, *2*, 257.
- (2) O'Keeffe, M.; Yaghi, O. M. *Chem. Rev.* **2011**, *112*, 675.
- (3) (a) Perles, J.; Iglesias, M.; Ruiz-Valero, C.; Snejko, N. *Chem. Commun.* **2003**, 346. (b) Perles, J.; Snejko, N.; Iglesias, M.; Monge, M. A. *J. Mater. Chem.* **2009**, *19*, 6504. (c) Perles, J.; Iglesias, M.; Martín-Luengo, M.-Á.; Monge, M. Á.; Ruiz-Valero, C.; Snejko, N. *Chem. Mater.* **2005**, *17*, 5837. (d) Mowat, J. P. S.; Miller, S. R.; Slawin, A. M. Z.; Seymour, V. R.; Ashbrook, S. E.; Wright, P. A. *Microporous Mesoporous Mater.* **2011**, *142*, 322. (e) Gandara, F.; Gomez-Lor, B.; Iglesias, M.; Snejko, N.; Gutierrez-Puebla, E.; Monge, A. *Chem. Commun.* **2009**, 2393. (f) Li, Y. T.; Cui, K. H.; Li, J.; Zhu, J. Q.; Wang, X.; Tian, Y. Q. *Chin. J. Inorg. Chem.* **2011**, *27*, 951. (g) Miller, S. R.; Wright, P. A.; Serre, C.; Loiseau, T.; Marrot, J.; Ferey, G. *Chem. Commun.* **2005**, 3850.
- (4) Kobayashi, S.; Mori, Y.; Yamashita, Y. In *Comprehensive Coordination Chemistry II*; McCleverty, J. A., Meyer, T. J., Eds.; Pergamon: Oxford, 2003.
- (5) (a) Tranchemontagne, D. J.; Park, K. S.; Furukawa, H.; Eckert, J.; Knobler, C. B.; Yaghi, O. M. *J. Phys. Chem. C* **2012**, *116*, 13143. (b) Furukawa, H.; Ko, N.; Go, Y. B.; Aratani, N.; Choi, S. B.; Choi, E.; Yazaydin, A. Ö.; Snurr, R. Q.; O'Keeffe, M.; Kim, J.; Yaghi, O. M. *Science* **2010**, *329*, 424.
- (6) (a) Ibarra, I. A.; Yang, S.; Lin, X.; Blake, A. J.; Rizkallah, P. J.; Nowell, H.; Allan, D. R.; Champness, N. R.; Hubberstey, P.; Schroder, M. *Chem. Commun.* **2011**, 47, 8304. (b) Webb, H. R.; Hardie, M. J.; Raston, C. L. *Chem.—Eur. J.* **2001**, *7*, 3616.
- (7) (a) Ibarra, I. A.; Lin, X.; Yang, S.; Blake, A. J.; Walker, G. S.; Barnett, S. A.; Allan, D. R.; Champness, N. R.; Hubberstey, P.; Schröder, M. *Chem.—Eur. J.* **2010**, *16*, 13671. (b) Dietzel, P. D. C.; Blom, R.; Fjellvag, H. *Dalton Trans.* **2006**, 2055.
- (8) Bernini, M. C.; Snejko, N.; Gutierrez-Puebla, E.; Monge, A. *CrystEngComm* **2011**, *13*, 1797.
- (9) (a) Bino, A.; Gibson, D. J. *Am. Chem. Soc.* **1982**, *104*, 4383. (b) Ardon, M.; Bino, A.; Jackson, W. G. *Polyhedron* **1987**, *6*, 181. (c) Ardon, M.; Bino, A.; Michelsen, K. J. *Am. Chem. Soc.* **1987**, *109*, 1986. (d) Ardon, M.; Bino, A.; Michelsen, K.; Pedersen, E.; Thompson, R. C. *Inorg. Chem.* **1997**, *36*, 4147. (e) Duan, L.; Fischer, A.; Xu, Y.; Sun, L. J. *Am. Chem. Soc.* **2009**, *131*, 10397. (f) Ruf, M.; Weis, K.; Vahrenkamp, H. J. *Am. Chem. Soc.* **1996**, *118*, 9288. (g) Kong, D.; Xie, Y. *Inorg. Chim. Acta* **2002**, *338*, 142. (h) Jüstel, T.; Bendix, J.; Metzler-Nolte, N.; Weyhermüller, T.; Nuber, B.; Wieghardt, K. *Inorg. Chem.* **1998**, *37*, 35.
- (10) APEX2; Bruker-AXS: Madison, WI, 2006.
- (11) SMART, v.5.04; Bruker-Siemens: Madison, WI, 1998.
- (12) SAINT, v.6.28A; Bruker-Siemens: Madison, WI, 1997.
- (13) SHELXTL, v.5.1; Bruker-Siemens: Madison, WI, 1998.
- (14) (a) Kresse, G.; Furthmüller, J. *Comput. Mater. Sci.* **1996**, *6*, 15. (b) Kresse, G.; Hafner, J. *Phys. Rev. B* **1993**, *47*, 558.

- (15) (a) Perdew, J. P.; Chevary, J. A.; Vosko, S. H.; Jackson, K. A.; Pederson, M. R.; Singh, D. J.; Fiolhais, C. *Phys. Rev. B* **1992**, *46*, 6671. (b) Perdew, J. P.; Wang, Y. *Phys. Rev. B* **1992**, *45*, 13244.
- (16) (a) Blöchl, P. E. *Phys. Rev. B* **1994**, *50*, 17953. (b) Kresse, G.; Joubert, D. *Phys. Rev. B* **1999**, *59*, 1758.
- (17) Momma, K.; Izumi, F. *J. Appl. Crystallogr.* **2011**, *44*, 1272.
- (18) Blatov, V. A.; Shevchenko, A. P.; V4.0 ed.; Samara State University: Samara, Russia, 2010.
- (19) *Infrared and Raman Spectra of Inorganic and Coordination Compounds*, 6th ed.; Nakamoto, K., Ed.; John Wiley & Sons, Inc.: Hoboken, NJ, 2009.
- (20) Harmon, K. M.; Southworth, B. A.; Mounts, P. A. *J. Mol. Struct.* **1993**, *296*, 69.
- (21) Price, E. A.; Robertson, W. H.; Diken, E. G.; Weddle, G. H.; Johnson, M. A. *Chem. Phys. Lett.* **2002**, *366*, 412.
- (22) Knop, O.; Hartley, J. M. *Can. J. Chem.* **1968**, *46*, 1446.
- (23) Belsky, A.; Hellenbrandt, M.; Karen, V. L.; Luksch, P. *Acta Crystallographica Section B* **2002**, *58*, 364.
- (24) (a) Gándara, F.; de la Peña-O'Shea, V. A.; Illas, F.; Snejko, N.; Proserpio, D. M.; Gutiérrez-Puebla, E.; Monge, M. A. *Inorg. Chem.* **2009**, *48*, 4707. (b) Bernini, M. C.; de la Peña-O'Shea, V. A.; Iglesias, M.; Snejko, N.; Gutiérrez-Puebla, E.; Brusau, E. V.; Narda, G. E.; Illas, F.; Monge, M. A. *Inorg. Chem.* **2010**, *49*, 5063. (c) Platero-Prats, A. E.; de la Peña-O'Shea, V. A.; Proserpio, D. M.; Snejko, N.; Gutiérrez-Puebla, E.; Monge, Á. *J. Am. Chem. Soc.* **2012**, *134*, 4762.
- (25) (a) Higuchi, K.; Onaka, M.; Izumi, Y. *Bull. Chem. Soc. Jpn.* **1993**, *66*, 2016. (b) North, M. *Tetrahedron: Asymmetry* **2003**, *14*, 147. (c) Thirupathi, B.; Patil, M. K.; Reddy, B. M. *Appl. Catal., A* **2010**, *384*, 147. (d) Benjamin, M. L.; John Wiley & Sons, Inc.: New York, 2010.
- (26) (a) Fujita, M.; Kwon, Y. J.; Washizu, S.; Ogura, K. *J. Am. Chem. Soc.* **1994**, *116*, 1151. (b) Evans, O. R.; Ngo, H. L.; Lin, W. J. *J. Am. Chem. Soc.* **2001**, *123*, 10395. (c) Schlichte, K.; Kratzke, T.; Kaskel, S. *Microporous Mesoporous Mater.* **2004**, *73*, 81. (d) Horike, S.; Dincă, M.; Tamaki, K.; Long, J. R. *J. Am. Chem. Soc.* **2008**, *130*, 5854. (e) Neogi, S.; Sharma, M. K.; Bharadwaj, P. K. *J. Mol. Catal. A: Chem.* **2009**, *299*, 1. (f) Sharma, M. K.; Singh, P. P.; Bharadwaj, P. K. *J. Mol. Catal. A: Chem.* **2011**, *342–343*, 6. (g) Wu, X.; Lin, Z.; He, C.; Duan, C. *New J. Chem.* **2012**, *36*, 161.
- (27) (a) D'Vries, R. F.; de la Peña-O'Shea, V. A.; Snejko, N.; Iglesias, M.; Gutiérrez-Puebla, E.; Monge, M. Á. *Cryst. Growth Des.* **2012**, *12*, 5535. (b) D'Vries, R. F.; Iglesias, M.; Snejko, N.; Gutiérrez-Puebla, E.; Monge, M. A. *Inorg. Chem.* **2012**, *51*, 11349.